Safety, Biodistribution, and Dosimetry of ^{123}I-IMPY: A Novel Amyloid Plaque–Imaging Agent for the Diagnosis of Alzheimer's Disease

Andrew B. Newberg[1], Nancy A. Wintering[1], Karl Plössl[1], John Hochold[1], Michael G. Stabin[2], Marianne Watson[3], Daniel Skovronsky[4], Christopher M. Clark[3], Mei-Ping Kung[1], and Hank F. Kung[1]

[1]Department of Radiology, University of Pennsylvania, Philadelphia, Pennsylvania; [2]Department of Radiology and Radiological Sciences, Vanderbilt University, Nashville, Tennessee; [3]Department of Neurology, Alzheimer's Disease Center, and Center of Excellence for Research on Neurodegenerative Diseases, University of Pennsylvania, Philadelphia, Pennsylvania; and [4]Avid Radiopharmaceuticals, Inc., Philadelphia, Pennsylvania

^{123}I-IMPY (6-iodo-2-(4′-dimethylamino-)phenyl-imidazo[1,2-a] pyridine) is a novel radiopharmaceutical that selectively binds to Alzheimer's disease (AD) amyloid plaques. As a first step toward validating this radiopharmaceutical as an imaging biomarker for AD, we measured the whole-body biokinetics and radiation dosimetry of ^{123}I-IMPY in AD patients and cognitively normal control subjects. The pharmacologic safety profile of the compound was simultaneously assessed. **Methods:** The sample included 9 subjects ranging in age from 44 to 80 y. Whole-body images were obtained for each subject (mean ± SD, 9.0 ± 3.2 scans per subject) for up to 48 h after the intravenous administration of 185 MBq (5 mCi) of ^{123}I-IMPY. The fraction of administered activity in 12 regions of interest was quantified from the attenuation-corrected geometric mean counts in conjugate views. Multiexponential functions were iteratively fit to each time–activity curve using a nonlinear, least-squares regression algorithm. These curves were numerically integrated to yield cumulated activity values for source organs. Radiation doses were then estimated with the MIRD technique. **Results:** The radiotracer had no pharmacologic effects (produced no changes in heart rate, blood pressure, or laboratory results) on any of the subjects. Radiation dosimetry estimates indicated that the dose-limiting organ was the gallbladder, which received an average of 0.135 mGy/MBq (range, 0.075–0.198 mGy/MBq). The effective dose equivalent and effective dose for ^{123}I-IMPY were 0.042 ± 0.003 mSv/MBq and 0.035 ± 0.001 mSv/MBq, respectively. The mean effective dose for ^{123}I-IMPY was similar to that for ^{111}In-diethylenetriaminepentaacetic acid (0.035 mGy/MBq), less than half that for ^{111}In-pentetreotide (0.81 mGy/MBq), and approximately twice that for ^{123}I-IMP (0.018 mGy/MBq). No significant differences were found between men and women or between AD patients and control subjects. **Conclusion:** ^{123}I-IMPY may be a safe radiotracer with appropriate biokinetics for imaging amyloid plaques in AD patients.

Key Words: neurology; ^{123}I-IMPY; amyloid plaque; Alzheimer's disease; dosimetry; SPECT

J Nucl Med 2006; 47:748–754

Alzheimer's disease (AD) is a brain disorder of the older population and is clinically characterized by progressive memory loss and a decline of cognitive function. However, a definitive diagnosis of AD can be established only by demonstrating the presence of abundant amyloid plaques (composed of aggregated amyloid-β peptide) and neurofibrillary tangles in the brain, usually at postmortem examination (*1,2*). A strong association of amyloid plaques with the pathogenesis of AD suggests that specific in vivo imaging agents targeting amyloid plaques may be clinically useful (*3,4*). The development of these imaging agents may open an avenue for following disease progression and may provide tools for monitoring therapeutic interventions to reduce the plaque burden in the AD brain. Amyloid plaque–imaging agents, if successfully developed, could also potentially be useful for early diagnosis of the disease.

The use of several ^{11}C- and ^{18}F-labeled tracers, that is, 6-OH-BTA-1 ([*N*-methyl-]2-(4′-methylaminophenyl)-6-hydroxybenzothiazole, also known as PIB (*5–7*)), SB-13 (4-*N*-methylamino-4′-hydroxystilbene (*8,9*)), and FDDNP (2-(1-{6-[(2-^{18}F-fluoroethyl)(methyl)amino]2-naphthyl}ethylidene)malononitrile (*10,11*)), has been reported for PET imaging of amyloid plaques in AD patients. Encouraging results with these tracers in AD patients suggest that the development of imaging agents for mapping amyloid plaques in the living human brain may be possible. However, PET, particularly with ^{11}C-labeled tracers, is not suitable for widespread community-based application because of the high cost of the studies, the requirement for a cyclotron, and the short half-life of the isotopes (20 min for ^{11}C). To overcome these problems, we have sought a much more inexpensive and widely available amyloid plaque–imaging radiopharmaceutical suitable for use with SPECT.

Received Oct. 12, 2005; revision accepted Feb. 6, 2006.

For correspondence or reprints contact: Andrew B. Newberg, 110 Donner Building, H.U.P., 3400 Spruce St., Philadelphia, PA 19104.
E-mail: andrew.newberg@uphs.upenn.edu

Currently, no SPECT agents for imaging specifically amyloid plaque have been evaluated in humans. As part of an effort to develop ^{123}I-labeled tracers suitable for SPECT, a series of radioiodinated probes based on various core structures were developed (*12–14*). Among dozens of iodinated ligands evaluated, 6-iodo-2-(4′-dimethylamino-)phenylimidazo[1,2-a]pyridine (IMPY; Fig. 1), showed the most desirable in vitro and in vivo characteristics (*15–17*). IMPY demonstrated a good binding affinity (inhibition constant, 15 nmol/L vs. ^{125}I-labeled 2-[4′-dimethylaminophenyl]-6-iodobenzothiazole as the ligand) for preformed synthetic amyloid-β peptide aggregates, and ^{125}I-IMPY displayed selective labeling of amyloid plaques both in postmortem sections of brain from AD patients and in transgenic mouse models of AD (*15*).

Ideal radiopharmaceuticals are safe, economical, and clinically effective. Initial studies of dosimetry and toxicology in rats and dogs by the National Institute on Aging suggested that nonradioactive IMPY had no substantial pharmacologic effects. Like any other radiopharmaceutical, the use of ^{123}I-IMPY in humans requires an estimation of its radiation dosimetry, that is, the amount of radiation energy deposited in each organ per unit dose of administered radioactivity (*18*). To perform this biodistribution and safety study, we submitted an Investigational New Drug Application to the Food and Drug Administration (investigational new drug 70,721).

In this paper, we present a detailed analysis of the biodistribution, dosimetry, and safety data of the use of ^{123}I-IMPY in humans. With these data obtained, future studies can be expanded into the clinical setting to test the usefulness of ^{123}I-IMPY in diagnosing and monitoring AD.

MATERIALS AND METHODS

Subject Accrual

The design was similar to several others that our laboratory has previously reported (*19–23*). The protocol was approved by the local Committee on Research Involving Humans and the U.S. Food and Drug Administration. Healthy volunteers were recruited through advertisements in local newspapers and by word of mouth from other volunteers. AD patients were referred from the Alzheimer's Disease Center and met the probable-AD criteria of the National Institute of Neurological and Communicative Disorders and Stroke and the Alzheimer Disease and Related Disorders Association (*24*). Medical histories were taken and physical examinations performed before inclusion. At the time of the study, none of the subjects had a known history of a health problem that could have significantly affected the biodistribution or elimination of the radioligand. All AD patients were taking donepezil and multivitamins. One patient was taking finasteride for the prostate, 1 patient was taking L-citalopram, 2 patients were taking 3-hydroxy-3-methylglutaryl coenzyme A reductase inhibitors, and 1 patient was taking a low dose of furosemide for mild hypertension. All urine drug screens and serum laboratory tests were performed to confirm that the individuals were healthy. The final sample included 9 subjects: 5 men and 4 women.

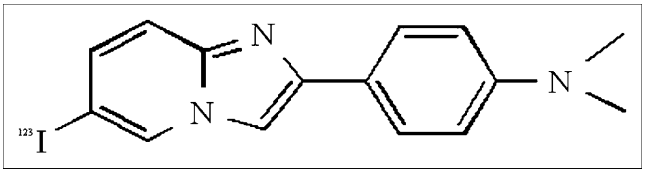

FIGURE 1. Chemical structure of ^{123}I-IMPY.

Clinical Assessment

The baseline clinical laboratory tests included a complete blood cell count with differential and tests of serum electrolytes and liver enzymes. Levels of creatinine, blood urea nitrogen, glucose, cholesterol, triglycerides, albumin, and total protein were also assayed. Routine urinalyses and urine toxicology screens were performed. The blood tests were repeated 4, 24, and, when possible, 48 h after administration of the radiopharmaceutical. The urine tests were repeated once after 24 h.

Electrocardiography was performed 20 min before injection of the radiopharmaceutical; 5, 10, 30, and 60 min after injection; and 24 h after injection. Vital signs (blood pressure, heart rate, and pulse oximetry) were taken about every 5 min from 20 min before injection to 60 min after injection.

Subject Preparation

On the morning of the first day of the study, intravenous access was obtained with the subjects lying supine on the imaging table. To block thyroid uptake, we gave Lugol's solution to the subjects 45 min before injection of ^{123}I-IMPY. Serum was obtained intravenously after the subjects had been lying supine for approximately 15 min. Electrocardiogram leads and a blood pressure cuff were placed on the subjects. Subjects were monitored for 20 min before injection of ^{123}I-IMPY and for up to 60 min after injection as already described.

Imaging Techniques

Linear attenuation was measured using a noncollimated transmission source prepared by dissolving about 1,000 MBq of ^{99m}Tc in a 1,600-mL sheet flood made of clear acrylic. Transmission scans were obtained and attenuation calculated using a previously described technique (*19*). For acquisition of emission images, 185 MBq (5 mCi) of the radiopharmaceutical were injected rapidly as a bolus through the indwelling intravenous catheter (the dose was determined by subtracting the activity remaining in the syringe after injection from the activity before injection). Whole-body images were acquired using a dual-head scanner (Prism 2000; Picker) previously calibrated for the ^{123}I isotope. Imaging was concentrated over the initial 6 h after injection (typically 6–10 scans), and the remaining images were acquired at approximately 24, 30, and 48 h after injection (Fig. 2). A mean of 9.0 ± 3.2 whole-body images were acquired. Each whole-body scan was acquired in a 256 × 1,024 matrix for either 10 or 20 min over a total excursion length of 214 cm.

Image Analysis

An operator drew regions of interest (ROIs) around 12 different organs or tissues and around the whole body. The regions were drawn on whichever scan showed the organ most clearly. Most organ boundaries were placed on the first whole-body scan. An abdominal ROI was drawn to include the entire abdomen except the liver. Thus, the abdominal ROI obtained the maximum activity in the entire gut, and it was assumed the activity found its way there via hepatobiliary excretion. Because of the blocking with

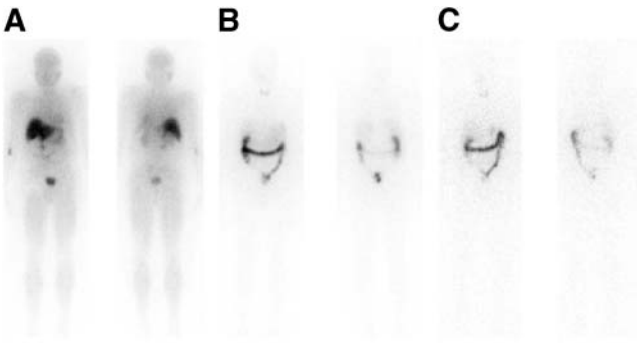

FIGURE 2. Representative anterior (left) and posterior (right) whole-body scans at 20 min (A), 26 h (B), and 48 h (C) after intravenous injection of ^{123}I-IMPY.

Lugol's solution, the thyroid was difficult to clearly visualize in most subjects, and therefore, the ROI representing the thyroid was large and stylized to reflect nonspecific activity in the region of the thyroid fossa. Because the kidneys were not visualized well in the anterior projection, the regions for them were placed by flipping the posterior ROIs.

Regardless of which scan the ROI originated from, it was cut and pasted into a single master set. Once the set was complete, the ROIs were transposed onto all the other images from the same patient, including the transmission scans. Occasionally, an operator had to move the entire set of ROIs to correct for repositioning errors between scans. In addition, the size of the ROIs for the urinary bladder sometimes had to be adjusted to account for normal changes in volume, with the regions always drawn to include all observable activity (the bladder was always clearly separated from any other areas of activity). The ROI for the body almost always required minor revisions to correct for subject movement, differences in pelvic tilt, and the position of the feet. Otherwise, the individual ROIs were rarely manipulated independently of the other regions in the set. An automated subroutine measured the number of counts in these ROIs.

Organ Activity Calculations

Attenuation corrections were applied using the experimentally measured ratio of counts in the transmission scans of the subjects on the imaging table and the forward-decay–corrected counts in the nonattenuated transmission scans through air.

Geometric means for each pair of decay- and attenuation-corrected conjugate ROIs were calculated by multiplying the net anterior counts by the net posterior counts and taking the square root of the product. Decay correction was necessary to compare each time point with the original whole-body activity level. The fraction of injected dose at each time point was then estimated by dividing the corrected geometric mean number of counts in each ROI by the net geometric mean number of counts in the initial whole-body image.

Organ Retention Functions

Time–activity curves were generated directly from the experimental data for the brain, gallbladder, heart, left kidney, liver, right lung, salivary glands, spleen, thyroid, urinary bladder, and the whole abdominal compartment excluding the urinary bladder. For this dataset, 1 or 2 exponential functions were iteratively fit to the time–activity curves using a nonlinear least-squares regression algorithm. These curves were numerically integrated to infinity to yield source organ cumulated activity values. Whole-body retention was estimated from the ROI encompassing the entire body. Urine was collected from each subject, and scintigraphic images of the collection jugs were obtained. However, when we discovered that difficulties in image acquisition or processing prevented the use of these data, urinary excretion was subsequently estimated from total-body clearance. The residence times for the urinary bladder, and thus the dose estimates that followed, were based on a theoretic bladder-voiding interval of 4.8 h, or 5 times a day (*25*).

Total fecal excretion was calculated as the maximum percentage injected activity in the gut at any image time during the study. The estimated gut radioactivity levels reached a maximum typically by about 24 h. Gallbladder residence times were calculated directly from the time–activity curves, with no accounting for routine voiding of the contents. Thus, gallbladder residence times (and radiation doses) are probably overestimates.

The percentages in the human organs were fit to 1- or 2-compartment exponential models using the SAAM II software (University of Washington). Time integrals of activity were calculated and converted to the number of disintegrations occurring in the source organs (*26*); these values were entered into the OLINDA/EXM 1.0 software (Vanderbilt University) using the adult male model, which calculates the values for other organs not measured directly using the regions. Excretion of activity was modeled by assuming that activity not accounted for in the measurements had been eliminated through the urine (a dynamic bladder model with a 4.8-h voiding interval was used to estimate the dose to the urinary bladder wall) and by assuming that the excretion was 75% urinary and 25% intestinal. This assumption was based on observations that the average percentage activity measured in the abdominal area, when activity in the kidneys, liver, and gallbladder was removed, was 23.4%, with an SD of 9.9%. The dose to the salivary glands was calculated separately (because this region is not defined in currently available phantoms and so is not in the OLINDA/EXM code) using the unit density sphere approximation in the OLINDA/EXM software.

Serum Metabolite Analysis

Heparinized blood samples (1–3 mL) were obtained from 3 healthy control subjects and 3 AD patients at various time points (2, 5, 10, 30, and 60 min) after an intravenous injection of ^{123}I-IMPY. The blood samples were centrifuged, and the obtained plasma samples were counted to determine total radioactivity. An equal volume (500 μL) of ethyl acetate was added to the plasma fraction in the presence of 20 μg of IMPY carrier to maximize extraction yield in the microcentrifuge tubes (1.3 mL). Extraction was repeated 3 times, and the combined EtOAc extraction and aqueous layer were counted separately to obtain the percentage of EtOAc extraction for each sample. To quantify the parent ^{123}I-IMPY nonmetabolized in the samples, EtOAc extracts were condensed and reconstituted in a small volume of MeOH for thin-layer chromatography analysis (silica gel, mobile phase: chloroform/EtOH/concentrated NH_3 = 8/1.5/drop). Under this thin-layer chromatography condition, ^{123}I-IMPY gave an R_f value of 0.8–0.9, whereas the metabolites showed lower R_f values, from which nonmetabolized ^{123}I-IMPY in EtOAc extract was quantified.

RESULTS

No changes in heart rate, blood pressure, physical examination findings, or laboratory values occurred

between the before- and after-injection time points. One subject reported 2 episodes of diarrhea, and 1 subject reported some dyspepsia. Both of these symptoms were self-limited. Both effects might have been related to the radiopharmaceutical, although the diarrhea was believed more likely related to a viral illness and the dyspepsia to the patient's having to lie down for prolonged periods during scanning.

Calculations of the residence times in each organ (Table 1) showed that the source organ with the longest residence time was the liver (mean, 1.91 h; range, 1.21–2.23 h). Table 2 lists the absorbed dose estimates for all subjects. The organ receiving the highest estimated dose across all subjects was the gallbladder, which received an estimated 0.135 mGy/MBq (range, 0.075–0.198 mGy/MBq). However, this dose may be an overestimate because the activity is assumed to be persistent even though the gallbladder must eliminate its contents when the subject eats. Ten organs were estimated to have radiation doses at or above 0.030 mGy/MBq: distal colon, 0.115 mGy/MBq; proximal colon, 0.104 mGy/MBq; bladder wall, 0.057 mGy/MBq; thyroid, 0.096 mGy/MBq; gallbladder wall, 0.052 mGy/MBq; kidneys, 0.054 mGy/MBq; small bowel, 0.053 mGy/MBq; heart wall, 0.135 mGy/MBq; salivary glands, 0.057 mGy/MBq; and liver, 0.045 mGy/MBq. The variability in organ-absorbed doses was reasonable, with substantially less variability associated with the mean effective dose equivalent and effective dose—0.042 ± 0.003 mSv/MBq and 0.035 ± 0.001 mSv/MBq, respectively.

Because tracer biodistribution in patients with AD might be different from that in control subjects, we analyzed whether any values differed between these 2 groups (Table 3). No significant difference was found between men and women. Although the groups were small, no significant difference in any organ or whole-body dosimetry estimate was found between AD patients and control subjects. The mean radiation dose estimate for the brain was slightly higher in the AD group, a finding that seems appropriate because the tracer target is AD-associated amyloid plaque, but the difference was not significant. SPECT brain scans obtained 2 h after injection demonstrated an approximately 20% increase (using simple ROIs) in cortical uptake in an AD patient, compared with a control subject. We are now determining the cerebral kinetics and most appropriate imaging times in a larger sample to adequately differentiate between AD patients and control subjects.

TABLE 1
^{123}I-IMPY Residence Times for All Subjects Taken Together

Source organ	Minimum	Maximum	Mean	SD
Brain	0.08	0.27	0.16	0.06
Salivary glands	0.12	0.29	0.19	0.06
Thyroid	0.05	0.13	0.09	0.03
Lungs	0.36	0.80	0.56	0.15
Heart	0.17	0.56	0.34	0.13
Liver	1.21	2.23	1.91	0.35
Gallbladder	0.15	0.78	0.46	0.23
Kidneys	0.32	0.78	0.54	0.18
Remainder	1.83	6.82	4.20	2.02

Data are hours.

The plasma concentration of ^{123}I-IMPY was studied in 3 healthy control subjects and 3 AD patients. All IMPY metabolites were polar (not extractable by organic solvent). The metabolism of ^{123}I-IMPY did not significantly differ between AD patients and the healthy control subjects. The amount of unchanged ^{123}I-IMPY decreased rapidly, with 73.4% ± 6.9% and 80% ± 8.0% remaining at 2 min after injection in AD patients and healthy control subjects, respectively. The amount of unchanged ^{123}I-IMPY at 30 and 60 min after ^{123}I-IMPY injection dropped to 22.2% ± 5.2% and 14.6% ± 3.8%, respectively, in AD patients and to 19.6% ± 6.9% and 9.3% ± 2.7%, respectively, in healthy control subjects.

DISCUSSION

^{123}I-IMPY appears to be pharmacologically safe in healthy volunteers and patients with AD, with no significant physiologic effects noted in laboratory measures, vital signs, or electrocardiograms. This apparent safety seems appropriate given the relatively small dose of ^{123}I-IMPY administered (approximately 21 pmol).

The data for this analysis were acquired using a protocol focusing on biodistribution and dosimetry. Radioactivity distributions were determined scintigraphically at approximately 9 time points. The time points were properly scheduled for estimating ^{123}I radiopharmaceutical doses. Early imaging (0–6 h after injection) was frequent, allowing for excellent mathematic modeling of the rapid-washout phase in the source organs and total body. Images were acquired until nearly 4 physical half-lives of ^{123}I had passed, allowing for accurate modeling of long-term retention and slow clearance. Accurately modeling the slow-clearance components minimizes the uncertainties associated with radiation doses to source organs (slowly clearing components usually account for most of the residence time in a source organ). From biologic models (based on image data), little of the ^{123}I appears to be permanently retained in the body or in any particular source organs. Even the kidneys, although continuing to accumulate radiation for, often, more than 6 h, eventually begin demonstrating a clearance phase over the final 24–48 h. Other limitations include the effect of the varying volumes of the bladder on overall counts and residence time calculations. We also used attenuation correction, which should help improve the accuracy of the counts provided but is also subject to error if improperly placed regions are used for calculating attenuation correction. Despite these limitations, the variability in residence times and radiation doses across all subjects was relatively low.

TABLE 2
Radiation Dose Estimates for Each Subject

Organ	Subject no., sex, group,* age (y), and weight (kg)										
	1, M, C, 54, 71.8	2, M, C, 80, 75.0	3, F, AD. 80, 52.3	4, M, C, 52, 79.5	5, F, AD, 71, 55.5	6, F, AD, 76, 68.2	7, M, C, 44, 59.1	8, F, C, 72, 75.5	9, F, AD, 76, 88.2	Average (67, 69.1)	SD (14, 11.8)
Adrenals	1.30E–02	1.23E–02	1.07E–02	1.39E–02	1.63E–02	1.28E–02	1.26E–02	9.78E–03	1.26E–02	1.27E–02	1.84E–03
Brain	5.66E–03	3.59E–03	2.68E–03	5.69E–03	8.75E–03	4.23E–03	4.42E–03	2.74E–03	4.18E–03	4.66E–03	1.87E–03
Breasts	3.74E–03	5.39E–03	3.15E–03	5.77E–03	6.62E–03	3.37E–03	4.09E–03	3.02E–03	4.88E–03	4.45E–03	1.28E–03
Gallbladder wall	1.45E–01	9.59E–02	1.45E–01	7.53E–02	1.28E–01	1.98E–01	1.98E–01	1.44E–01	8.86E–02	1.35E–01	4.40E–02
Lower large intestine wall	1.15E–01	1.16E–01	1.14E–01	1.16E–01	1.16E–01	1.14E–01	1.14E–01	1.14E–01	1.16E–01	1.15E–01	1.00E–03
Small intestine	4.50E–02	4.60E–02	4.36E–02	4.65E–02	4.75E–02	4.43E–02	4.53E–02	4.34E–02	4.58E–02	4.53E–02	1.35E–03
Stomach wall	1.04E–02	1.18E–02	8.99E–03	1.25E–02	1.38E–02	9.82E–03	1.08E–02	8.83E–03	1.14E–02	1.09E–02	1.63E–03
Upper large intestine wall	1.04E–01	1.04E–01	1.02E–01	1.04E–01	1.06E–01	1.03E–01	1.04E–01	1.02E–01	1.04E–01	1.04E–01	1.22E–03
Heart wall	1.94E–02	3.66E–02	1.88E–02	3.68E–02	5.18E–02	3.96E–02	3.83E–02	2.90E–02	2.59E–02	3.29E–02	1.06E–02
Kidneys	7.06E–02	4.66E–02	5.36E–02	5.67E–02	6.35E–02	7.73E–02	4.44E–02	3.68E–02	3.73E–02	5.41E–02	1.43E–02
Liver	5.10E–02	3.12E–02	4.25E–02	3.98E–02	5.14E–02	5.24E–02	5.22E–02	4.11E–02	4.54E–02	4.52E–02	7.26E–03
Lungs	1.64E–02	2.02E–02	2.10E–02	2.08E–02	2.64E–02	1.99E–02	1.56E–02	1.44E–02	1.45E–02	1.88E–02	3.93E–03
Muscle	7.10E–03	8.49E–03	6.09E–03	8.90E–03	9.62E–03	6.40E–03	7.22E–03	5.98E–03	8.16E–03	7.55E–03	1.30E–03
Ovaries	2.64E–02	2.81E–02	2.54E–02	2.84E–02	2.86E–02	2.54E–02	2.63E–02	2.53E–02	2.78E–02	2.69E–02	1.37E–03
Pancreas	1.33E–02	1.31E–02	1.12E–02	1.42E–02	1.68E–02	1.33E–02	1.39E–02	1.07E–02	1.32E–02	1.33E–02	1.75E–03
Red marrow	7.78E–03	8.99E–03	6.73E–03	9.50E–03	1.03E–02	7.10E–03	7.80E–03	6.56E–03	8.68E–03	8.16E–03	1.29E–03
Osteogenic cells	1.46E–02	2.07E–02	1.12E–02	2.21E–02	2.39E–02	1.10E–02	1.50E–02	1.11E–02	1.96E–02	1.66E–02	5.08E–03
Salivary glands	4.51E–02	5.42E–02	6.62E–02	5.08E–02	8.61E–02	4.73E–02	3.82E–02	8.73E–02	3.70E–02	5.69E–02	1.90E–02
Skin	3.36E–03	4.55E–03	2.62E–03	4.86E–03	5.26E–03	2.65E–03	3.43E–03	2.60E–03	4.34E–03	3.74E–03	1.03E–03
Spleen	8.43E–03	9.63E–03	6.81E–03	1.05E–02	1.16E–02	7.80E–03	7.77E–03	6.07E–03	8.76E–03	8.60E–03	1.76E–03
Testes	5.10E–03	6.68E–03	4.32E–03	6.90E–03	6.92E–03	4.14E–03	5.01E–03	4.32E–03	6.40E–03	5.53E–03	1.18E–03
Thymus	4.85E–03	7.73E–03	4.03E–03	8.13E–03	9.50E–03	4.82E–03	5.84E–03	4.28E–03	6.67E–03	6.21E–03	1.92E–03
Thyroid	9.91E–02	1.36E–01	5.46E–02	7.00E–02	7.64E–02	1.14E–01	1.04E–01	1.26E–01	8.53E–02	9.62E–02	2.69E–02
Urinary bladder wall	6.58E–02	4.94E–02	7.12E–02	4.46E–02	3.32E–02	7.40E–02	5.61E–02	6.83E–02	5.16E–02	5.71E–02	1.37E–02
Uterus	1.86E–02	1.92E–02	1.78E–02	1.93E–02	1.88E–02	1.80E–02	1.79E–02	1.76E–02	1.91E–02	1.85E–02	6.61E–04
Total body	9.79E–03	1.07E–02	8.46E–03	1.14E–02	1.27E–02	9.24E–03	9.90E–03	8.24E–03	1.06E–02	1.01E–02	1.42E–03
Effective dose equivalent	4.35E–02	4.08E–02	4.13E–02	3.83E–02	4.34E–02	4.78E–02	4.51E–02	4.17E–02	3.79E–02	4.22E–02	3.15E–03
Effective dose	3.58E–02	3.72E–02	3.31E–02	3.45E–02	3.60E–02	3.69E–02	3.54E–02	3.56E–02	3.45E–02	3.54E–02	1.27E–03

*Group C = control group.
Data are mGy/MBq. Effective dose equivalent and effective dose are mSv/MBq.

TABLE 3
Comparison of Organ Radiation Dose Estimates Between Control Subjects and AD Patients

Organ	AD patients		Control subjects	
	Average	SD	Average	SD
Adrenals	1.31E–02	2.33E–03	1.23E–02	1.54E–03
Brain	4.96E–03	2.63E–03	4.42E–03	1.29E–03
Breasts	4.51E–03	1.61E–03	4.40E–03	1.15E–03
Gallbladder wall	1.40E–01	4.54E–02	1.32E–01	4.79E–02
LLI wall	1.15E–01	1.15E–03	1.15E–01	1.00E–03
Small intestine	4.53E–02	1.73E–03	4.52E–02	1.18E–03
Stomach wall	1.10E–02	2.12E–03	1.09E–02	1.41E–03
ULI wall	1.04E–01	1.71E–03	1.04E–01	8.94E–04
Heart wall	3.40E–02	1.47E–02	3.20E–02	7.93E–03
Kidneys	5.79E–02	1.68E–02	5.10E–02	1.30E–02
Liver	4.79E–02	4.76E–03	4.31E–02	8.68E–03
Lungs	2.05E–02	4.88E–03	1.75E–02	2.86E–03
Muscle	7.57E–03	1.64E–03	7.54E–03	1.17E–03
Ovaries	2.68E–02	1.65E–03	2.69E–02	1.31E–03
Pancreas	1.36E–02	2.33E–03	1.30E–02	1.38E–03
Red marrow	8.20E–03	1.63E–03	8.13E–03	1.15E–03
Osteogenic cells	1.64E–02	6.39E–03	1.67E–02	4.58E–03
Salivary glands	5.92E–02	2.17E–02	5.51E–02	1.90E–02
Skin	3.72E–03	1.31E–03	3.76E–03	9.29E–04
Spleen	8.74E–03	2.06E–03	8.48E–03	1.71E–03
Testes	5.45E–03	1.42E–03	5.60E–03	1.13E–03
Thymus	6.26E–03	2.43E–03	6.17E–03	1.71E–03
Thyroid	8.26E–02	2.46E–02	1.07E–01	2.57E–02
UB wall	5.75E–02	1.90E–02	5.68E–02	1.02E–02
Uterus	1.84E–02	6.24E–04	1.85E–02	7.60E–04
Total body	1.03E–02	1.86E–03	1.00E–02	1.18E–03
Effective dose equivalent	4.26E–02	4.14E–03	4.19E–02	2.60E–03
Effective dose	3.51E–02	1.67E–03	3.57E–02	9.75E–04

LLI = lower large intestine; ULI = upper large intestine; UB = urinary bladder.

Control subjects and AD patients do not significantly differ. Data are mGy/MBq. Effective dose equivalent and effective dose are mSv/MBq.

The subjects underwent thyroid blocking before administration of the ^{123}I-IMPY. Effective thyroid blocking should, in theory, reduce thyroid uptake of unbound iodide to negligible levels. In addition, during drawing of the ROIs, miniscule accumulations of radioactivity were visualized in the thyroid and in the region referred to as external genitalia in all subjects. Because the ROI counts were not background subtracted during image quantification, the counts in these 2 regions may simply have been soft-tissue background activity. The mean value for thyroid residence time (0.09 h) was by far the shortest of the residence times calculated (by a factor of about 2). In addition, the estimates of dose to the gallbladder wall are overestimates. For gallbladder contents, we assumed that no periodic voiding of the gallbladder occurred after the injection. Clearly, because radioactivity reached the gut lumen, voiding of the gallbladder had occurred.

In the 9 subjects studied, estimates of radiation-related risk (effective dose) were similar to those of other nuclear medicine procedures (on a per-unit-of-administered-activity basis) such as ^{111}In-pentetreotide (0.081 mSv/MBq), ^{111}In-diethylenetriaminepentaacetic acid (0.035 mSv/MBq), and ^{18}F-FDG (0.024 mSv/MBq) (*27*) and approximately twice that of ^{123}I-IMP (0.018 mGy/MBq). The effective doses for other iodinated radiopharmaceuticals are also available for comparison: 2β-carbomethoxy-3β-(4-iodophenyl)-*N*-(3-fluoropropyl)nortropane (0.024 mSv/MBq) (*28*) and iodobenzamide (0.034 mSv/MBq) (*29*). These values are comparable to the estimate of effective dose for the adult male in this study: 0.035 mSv/MBq.

CONCLUSION

There has been considerable interest in the development of selective tracers for imaging amyloid plaques in patients with suspected AD. Several new PET tracers appear able to detect amyloid plaques. The ^{11}C-based Pittsburgh Compound B has been shown in postmortem studies to bind to amyloid plaques in the brains of AD patients. Furthermore, the initial study on 16 patients with early, mild AD showed increased binding in brain structures that typically have significant amyloid plaques, such as the temporoparietal and frontal regions, compared with areas such as the cerebellum. This study also correlated uptake of Pittsburgh Compound B with uptake of ^{18}F-FDG and found a significant negative correlation between the two in AD patients. However, PET tracers tend to be difficult to produce, difficult to use clinically, and costly. An iodinated compound that is selective for amyloid plaques and suitable for SPECT is more likely to be cost effective and, ultimately, easier to use clinically. For these reasons, we have developed ^{123}I-IMPY, which can be produced from prepared kits for potentially easier clinical use and lower overall cost.

This study measured the whole-body biodistribution of ^{123}I-IMPY and determined initial safety data, including laboratory values, vital signs, and electrocardiograms. The effective dose equivalent and effective dose parameters can compare the radiologic risk associated with low radiation exposures, and ^{123}I-IMPY compares well with other radiopharmaceuticals. Overall, these results, in addition to the clinical and laboratory data, indicate that ^{123}I-IMPY may be a safe agent for imaging amyloid plaque in patients with AD.

ACKNOWLEDGMENTS

This study was partially supported by NIH grants RO1-EB00360, R21-AG021868, and AG010124 and by a generous contribution from the James Previti Family Fund.

REFERENCES

1. Ginsberg SD, Schmidt ML, Crino PB, Eberwine JH, Lee VM-Y, Trojanowski JQ. Molecular pathology of Alzheimer's disease and related disorders. In: Peters A, Morrison JH, eds. *Cerebral Cortex: Neurodegenerative and Age-Related*

Changes in Structure and Function of Cerebral Cortex. New York, NY: Kluwer Academic/Plenum; 1999:603–654.
2. Selkoe DJ. The origins of Alzheimer disease: A is for amyloid. *JAMA.* 2000;283:1615–1617.
3. Selkoe DJ. Imaging Alzheimer's amyloid. *Nat Biotechnol.* 2000;18:823–824.
4. Hardy J, Selkoe DJ. The amyloid hypothesis of Alzheimer's disease: progress and problems on the road to therapeutics. *Science.* 2002;297:353–356.
5. Mathis CA, Wang Y, Holt DP, et al. Synthesis and evaluation of ^{11}C-labeled 6-substituted 2-arylbenzothiazoles as amyloid imaging agents. *J Med Chem.* 2003;46:2740–2754.
6. Mathis CA, Wang Y, Klunk WE. Imaging β-amyloid plaques and neurofibrillary tangles in the aging human brain. *Curr Pharm Des.* 2004;10:1469–1492.
7. Klunk WE, Engler H, Nordberg A, et al. Imaging brain amyloid in Alzheimer's disease with Pittsburgh Compound-B. *Ann Neurol.* 2004;55:306–319.
8. Ono M, Kung M-P, Hou C, Kung HF. Benzofuran derivatives as Aβ-aggregate-specific imaging agents for Alzheimer's disease. *Nucl Med Biol.* 2002;29:633–642.
9. Wilson A, Nobrega J, Houle S, et al. Radiosynthesis and evaluation of potential β-amyloid imaging radiotracer for PET [abstract]. *J Labelled Compds Radiopharm.* 2003;46(suppl):S61.
10. Agdeppa ED, Kepe V, Shoghi-Jadid K, et al. In vivo and in vitro labeling of plaques and tangles in the brain of an Alzheimer's disease patient: a case study [abstract]. *J Nucl Med.* 2001;42(suppl):65P.
11. Shoghi-Jadid K, Small GW, Agdeppa ED, et al. Localization of neurofibrillary tangles and beta-amyloid plaques in the brains of living patients with Alzheimer disease: binding characteristics of radiofluorinated 6-dialkylamino-2-naphthylethylidene derivatives as positron emission tomography imaging probes for beta-amyloid plaques in Alzheimer disease. *Am J Geriatr Psychiatry.* 2002;10:24–35.
12. Zhuang Z-P, Kung M-P, Hou C, et al. Radioiodinated styrylbenzenes and thioflavins as probes for amyloid aggregates. *J Med Chem.* 2001;44:1905–1914.
13. Kung HF, Lee C-W, Zhuang ZP, et al. Novel stilbenes as probes for amyloid plaques. *J Am Chem Soc.* 2001;123:12740–12741.
14. Lee C-W, Kung M-P, Hou C, Kung HF. Dimethylamino-fluorenes: ligands for detecting β amyloid plaques in the brain. *Nucl Med Biol.* 2003;30:573–580.
15. Kung MP, Hou C, Zhuang ZP, et al. Characterization of IMPY as a potential imaging agent for b-amyloid plaques in double transgenic PSAPP mice. *Eur J Nucl Med Mol Imaging.* 2004;31:1136–1145.
16. Kung MP, Hou C, Zhuang ZP, et al. IMPY: an improved thioflavin-T derivative for in vivo labeling of β-amyloid plaques. *Brain Res.* 2002;956:202–210.
17. Zhuang ZP, Kung MP, Wilson A, et al. Structure-activity relationship of imidazo[1,2-a]pyridines as ligands for detecting beta-amyloid plaques in the brain. *J Med Chem.* 2003;46:237–243.
18. Sorenson JA, Phelps ME. Internal radiation dosimetry. In: *Physics in Nuclear Medicine.* 2nd ed. Philadelphia, PA: W.B. Saunders; 1987:197–218.
19. Newberg AB, Plössl K, Mozley PD, et al. Biodistribution and imaging with I-123 ADAM: a serotonin transporter imaging agent. *J Nucl Med.* 2004;45:834–841.
20. Mozley PD, Zhu XW, Kung HF, et al. The dosimetry of 3-iodo-Schering 23390: quantification of the radiation burden to healthy humans. *J Nucl Med.* 1993;34:208–213.
21. Mozley PD, Stubbs JS, Kung HF, et al. Biodistribution and dosimetry of I-123 IBF: a potent radioligand for imaging the D2 dopamine receptor. *J Nucl Med.* 1993;34:1910–1917.
22. Mozley PD, Stubbs JB, Kim H-J, et al. Dosimetry of a D2/D3 dopamine receptor antagonist that can be used with PET or SPECT. *J Nucl Med.* 1995;36:1322–1331.
23. Mozley PD, Stubbs JB, Kim H-J, et al. Dosimetry of an iodine-123-labeled tropane to image dopamine transporters. *J Nucl Med.* 1996;37:151–159.
24. McKhann G, Drachman D, Folstein M, et al. Clinical diagnosis of Alzheimer's disease: report of the NINCDS-ADRDA Work Group under the auspices of Department of Health and Human Services Task Force on Alzheimer' Disease. *Neurology.* 1984;34:939–944.
25. Cloutier RJ, Smith SA, Watson EE, et al. Dose to the fetus from radionuclides in the bladder. *Health Phys.* 1973;25:147–161.
26. Loevinger R, Budinger TF, Watson EE. *MIRD Primer for Absorbed Dose Calculations.* New York, NY: Society of Nuclear Medicine; 1988.
27. Toohey RE, Stabin MG. Comparative analysis of dosimetry parameters for nuclear medicine. In: Proceedings of the 6th International Radiopharmaceutical Dosimetry Symposium; May 7–10, 1996; Gatlinburg, TN.
28. Booij J, Busemann SE, Stabin MG, et al. Human biodistribution and dosimetry of [^{123}IFP-CIT: a potent radioligand for imaging the dopamine transporters. *Eur J Nucl Med.* 1998;25:24–30.
29. Verhoeff NP, Sokole EB, Stabin M, et al. Dosimetry of iodine-123 iobenzamide in healthy volunteers. *Eur J Nucl Med.* 1993;20:747–752.